Penetration Through Slots in Conducting Cylinders—Part 2: TM Case

John D. Shumpert, *Student Member, IEEE*, and Chalmers M. Butler, *Fellow, IEEE*

***Abstract*— Three methods for determining the penetration through small apertures in closed conducting surfaces are outlined and their salient features discussed. These methods are designated: 1) the scatterer method; 2) the short-circuit current method; and 3) the equivalent current method. They are implemented by integral equation techniques but are amenable to differential equation or hybrid methods. Procedures for applying each method are outlined as are schemes for repairing singular equations rendered invalid by the presence of false resonances. Reasons for inaccuracies in the three methods are also delineated. Data determined for a given structure by all three methods are presented and numerical examples that illustrate important features of the methods and their relative accuracies are described. In Part 1, the TE (to cylinder axis) case is presented. In this part of the paper is found an outline of the integral equation formulation and numerical scheme needed to accurately determine the field that penetrates through a slot in a conducting cylinder, excited by an axially independent TM source.**

***Index Terms*—Apertures, electromagnetic coupling, numerical analysis.**

I. Introduction

PART 1 outlined the integral equation formulation and numerical scheme needed to accurately determine the field that penetrates through a slot in a conducting cylinder, excited by an axially independent TE (to cylinder axis) source [1]. Data determined for a given structure by three methods are presented and numerical examples that illustrate important observations about the methods are described. The reader is referred to the first paper for a bibliography concerning penetration of fields through slots in conducting surfaces.

Integral equations are derived that can be solved for equivalent currents from which the TM penetrated field can be determined. These equations are developed in Section II for the: 1) scatterer method; 2) short-circuit current method; and 3) equivalent current method. Procedures for applying each method are outlined and the limitations of each method are discussed, as are schemes for repairing singular equations rendered invalid by the presence of false resonances. In Section III, moment-method solutions are developed for the integral equations derived in Section II. Data determined for a given structure by all three methods are presented and numerical examples that illustrate important observations about the methods are described in Section IV.

Manuscript received December 4, 1995; revised September 8, 1997. This work was supported by the U.S. Army Research Office under Grant DAAL03-92-G-0376 and by the National Science Foundation through its Graduate Fellowship Program.

J. D. Shumpert was with the Department of Electrical and Computer Engineering, Clemson University, Clemson, SC 29634 USA. He is now with the Radiation Laboratory, Department of Electrical Engineering and Computer Science, University of Michigan, Ann Arbor, MI 48109 USA. He

C. M. Butler is with the Department of Electrical and Computer Engineering, Clemson University, Clemson, SC, 29634 USA.

Publisher Item Identifier S 0018-926X(98)08880-2.

II. Formulation of Integral Equations

Three methods for determining penetrated field through slots in conducting cylinders are outlined and procedures for applying the methods are delineated in detail in Part 1. These methods include the *scatterer method*, *short-circuit current method*, and *equivalent current method*. We include here only the final equations for the TM case.

A. Scatterer Method

In the scatterer method, the body is treated as a scatterer and the total field everywhere is determined as the sum of the incident field produced by a known source and the scattered field contributed by the current induced on the body. Consider the slotted cylinder in [1, Fig. 2]. The cylinder is excited by an incident time harmonic ($e^{j\omega t}$) plane wave propagating in a direction normal to the z axis with its electric field parallel to the axis (TM_z), which induces an electric current $\mathbf{J} = J_z\hat{\mathbf{z}}$ with a z component only. The following electric field integral equation (EFIE) can be formulated to determine the induced current J_z on the scatterer

$$\frac{k\eta}{4}\int_{C_S} J_z(\boldsymbol{\rho}')H_0^{(2)}(k|\boldsymbol{\rho}-\boldsymbol{\rho}'|)\,dl' = E_z^i(\boldsymbol{\rho}), \boldsymbol{\rho}\in C_S \qquad (1)$$

where C_S is the contour of the cylindrical conductor. Note that since all quantities are z-invariant and the induced electric current is z directed, $\nabla_s\cdot\mathbf{J}(\boldsymbol{\rho})$ of (3) in [1] is zero. The total electric field everywhere is computed as the sum of the scattered field produced by the induced electric current found in (1) and the incident electric field given by $\mathbf{E}^i = \hat{\mathbf{z}}E_o^i e^{jk(x\cos\phi^i + y\sin\phi^i)}$, which impinges upon the cylinder along a ray in the $\hat{\mathbf{k}} = -(\cos\phi^i\hat{\mathbf{x}} + \sin\phi^i\hat{\mathbf{y}})$ direction defined by an angle ϕ^i with respect to the x axis.

B. Short-Circuit Current Method

The short-circuit current method is based on a field equivalence theorem due to Schelkunoff [2] that allows one to

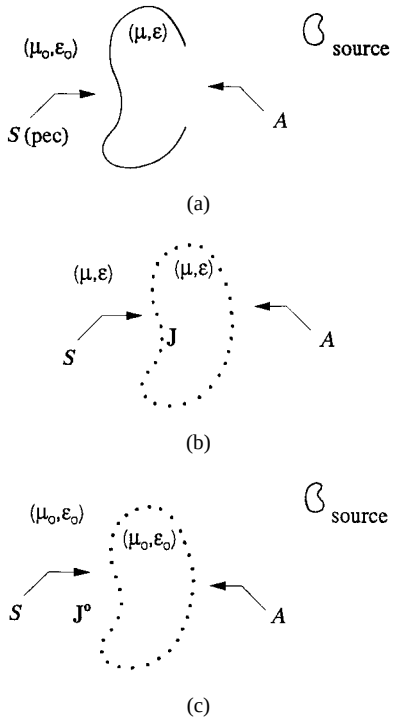

Fig. 1. Illustrations for the equivalent current method. (a) Original structure. (b) Interior equivalent model. (c) Exterior equivalent model.

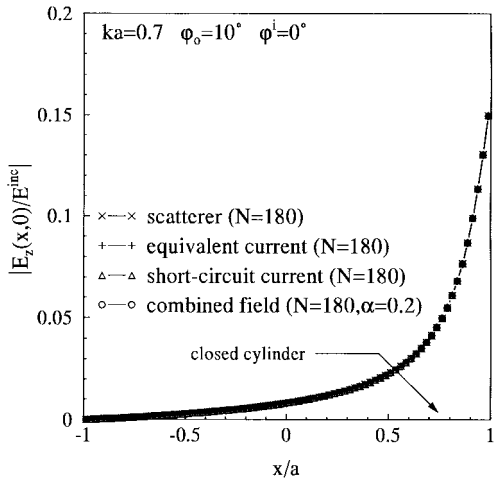

Fig. 2. Magnitude of axially directed (normalized) electric field on x axis of slotted circular cylinder excited by TM$_z$ plane wave [$ka = 0.7$, $\phi_o = 10°$, $\phi^i = 0°$].

replace the effect of an aperture in the surface of a body with equivalent "impressed" currents in the aperture. The short-circuit current over the conductor and shorted aperture can be found from

$$\frac{k\eta}{4}\int_{C_S+C_A} J_z^{\rm sc}(\boldsymbol{\rho}')H_0^{(2)}(k|\boldsymbol{\rho}-\boldsymbol{\rho}'|)\,dl' = E_z^i(\boldsymbol{\rho}), \quad \boldsymbol{\rho}\in C_S+C_A \quad (2)$$

where E_z^i is the z component of $\mathbf{E}^i$, C_S is the contour of the conductor and C_A is the contour of the shorted aperture. Note that (1) and (2) differ only in the inclusion of the shorted aperture. To overcome problems caused by false interior resonances, one may replace (2) by the corresponding combined field integral equation

$$\begin{aligned}\frac{1}{2}J_z^{\rm sc}(\boldsymbol{\rho}) &- \frac{k}{4j}\int_{C_S+C_A} J_z^{\rm sc}(\boldsymbol{\rho}')\cos\theta H_1^{(2)}(k|\boldsymbol{\rho}-\boldsymbol{\rho}'|)\,dl' \\ &+ \frac{\alpha k}{4}\int_{C_S+C_A} J_z^{\rm sc}(\boldsymbol{\rho}')H_0^{(2)}(k|\boldsymbol{\rho}-\boldsymbol{\rho}'|)\,dl' \\ &= H_l^i(\boldsymbol{\rho}) + \frac{\alpha}{\eta}E_z^i(\boldsymbol{\rho}), \quad \boldsymbol{\rho}\in C_S+C_A \end{aligned} \quad (3)$$

with $H_l^i(\boldsymbol{\rho})$ defined as

$$H_l^i(\boldsymbol{\rho}) = \hat{\mathbf{l}}\cdot(\hat{\mathbf{k}}\times\hat{\mathbf{z}})\frac{E_o^i}{\eta}e^{jk(x\cos\phi^i+y\sin\phi^i)} \quad (4)$$

where $\hat{\mathbf{l}}$ is a unit vector in the transverse plane tangential to the contour and $\hat{\mathbf{k}}$ is the direction of propagation of the incident field. $\cos\theta = \hat{\mathbf{u}}\cdot\hat{\mathbf{n}}$ with $\hat{\mathbf{u}} = (\boldsymbol{\rho}-\boldsymbol{\rho}')/|\boldsymbol{\rho}-\boldsymbol{\rho}'|$, $\hat{\mathbf{n}}$ is the outward normal depicted in [1, Fig. 1] located at the field point defined by the vector $\boldsymbol{\rho}$, and α is a multiplicative parameter that is usually chosen to be in the range $0.2 \le \alpha \le 1$ [3]. In the event that the radius of curvature of a surface is discontinuous at $\boldsymbol{\rho}$, $\frac{1}{2}J_z^{\rm sc}$ must be replaced by $\frac{\beta}{2\pi}J_z^{\rm sc}$ where β is the angle of the indentation or protrusion of the surface at $\boldsymbol{\rho}$ as defined in [4].

Using as a source the negative of the aperture short-circuit current on the aperture found by solving (2) or (3), we determine the induced current $\mathbf{J} = J_z\hat{\mathbf{z}}$ on the cylindrical scatterer as the solution of

$$\begin{aligned}\frac{k\eta}{4}&\int_{C_S} J_z(\boldsymbol{\rho}')H_0^{(2)}(k|\boldsymbol{\rho}-\boldsymbol{\rho}'|)\,dl' \\ &= -\frac{k\eta}{4}\int_{C_A} J_z^{\rm imp}(\boldsymbol{\rho}')H_0^{(2)}(k|\boldsymbol{\rho}-\boldsymbol{\rho}'|)\,dl', \quad \boldsymbol{\rho}\in C_S \end{aligned} \quad (5)$$

in which the right-hand side is the z component of the known E-field excitation due to $\mathbf{J}^{\rm imp}(=-\mathbf{J}^{\rm sc})$ on C_A. The penetrated electric field is $\hat{\mathbf{z}}E_z^{\rm pen}$ where

$$\begin{aligned}E_z^{\rm pen}(\boldsymbol{\rho}) = &-\frac{k\eta}{4}\int_{C_S} J_z(\boldsymbol{\rho}')H_0^{(2)}(k|\boldsymbol{\rho}-\boldsymbol{\rho}'|)\,dl' \\ &-\frac{k\eta}{4}\int_{C_A} J_z^{\rm imp}(\boldsymbol{\rho}')H_0^{(2)}(k|\boldsymbol{\rho}-\boldsymbol{\rho}'|)\,dl' \end{aligned} \quad (6)$$

where in (6) both J_z and $J_z^{\rm imp}$ are known currents. $J_z^{\rm imp}$ is known from the solution of (2) or (3) and J_z is known from the solution of (5).

C. Equivalent Current Method

In the equivalent current method, we introduce an electromagnetic model valid in the interior region and another valid in the exterior and we construct fields which satisfy the conditions that the tangential component of electric field be zero on the surfaces of the conducting body and that both the electric and magnetic fields be continuous through the aperture [5]. Of course, the field of the exterior model must satisfy the radiation condition. The interior and exterior models are suggested in Fig. 1. In the *interior* equivalent model of Fig. 1(b), we remove the conductor and place electric current $\mathbf{J}$ over the combined surface $(\mathcal{S}+\mathcal{A})$. All space of this model is filled with material characterized by that of the original interior

region (μ, ε). For the *exterior* equivalent model of Fig. 1(c), we place equivalent electric currents $\mathbf{J}^o$ over $\mathcal{A}$ *and* over $\mathcal{S}$ and fill all space with material characterized by (μ_o, ε_o). Neither $\mathbf{J}$ nor $\mathbf{J}^o$ is a physical current as is that in the scatterer and short-circuit current method. The fields of the two models must satisfy

$$\mathcal{E}_{\tan}[\mathbf{J};\mathbf{r};\mathcal{S}+\mathcal{A}] = \mathbf{0}, \quad \mathbf{r} \in \mathcal{S} \tag{7}$$

$$\mathcal{E}^o_{\tan}[\mathbf{J}^o;\mathbf{r};\mathcal{S}+\mathcal{A}] + \mathbf{E}^i_{\tan}(\mathbf{r}) = \mathbf{0}, \quad \mathbf{r} \in \mathcal{S} \tag{8}$$

$$\mathcal{E}_{\tan}[\mathbf{J};\mathbf{r};\mathcal{S}+\mathcal{A}] = \mathcal{E}^o_{\tan}[\mathbf{J}^o;\mathbf{r};\mathcal{S}+\mathcal{A}] + \mathbf{E}^i_{\tan}(\mathbf{r}), \quad \mathbf{r} \in \mathcal{A} \tag{9}$$

$$\mathcal{H}^-_{\tan}[\mathbf{J};\mathbf{r};\mathcal{S}^- + \mathcal{A}^-] = \mathcal{H}^{o^+}_{\tan}[\mathbf{J}^o;\mathbf{r};\mathcal{S}^+ + \mathcal{A}^+] + \mathbf{H}^i_{\tan}(\mathbf{r}), \quad \mathbf{r} \in \mathcal{A} \tag{10}$$

where $\mathcal{E}[\mathbf{J};\mathbf{r};\Sigma]$ and $\mathcal{H}[\mathbf{J};\mathbf{r};\Sigma]$ can be expressed in terms of potentials as

$$\mathcal{E}[\mathbf{J};\mathbf{r};\Sigma] = -j\omega\mathbf{A}(\mathbf{r}) - \nabla\Phi(\mathbf{r}) \tag{11}$$

and

$$\mathcal{H}[\mathbf{J};\mathbf{r};\Sigma] = \frac{1}{\mu}\nabla\times\mathbf{A}(\mathbf{r}) = \iint_{\Sigma} \mathbf{J}(\mathbf{r}')\times\nabla'_s G(\mathbf{r};\mathbf{r}')\,dS, \quad \mathbf{r}\notin\mathbf{r}' \tag{12}$$

with

$$\begin{aligned} \mathbf{A}(\mathbf{r}) &= \mu\iint_{\Sigma}\mathbf{J}(\mathbf{r}')G(\mathbf{r};\mathbf{r}')\,dS' \\ \Phi(\mathbf{r}) &= \frac{j\eta}{k}\iint_{\Sigma}(\nabla'_s\cdot\mathbf{J}(\mathbf{r}'))\,G(\mathbf{r};\mathbf{r}')\,dS'. \end{aligned} \tag{13}$$

$G(\mathbf{r};\mathbf{r}')$ is the free-space Green's function, $\eta = \sqrt{\mu/\varepsilon}$, $k = \omega\sqrt{\mu\varepsilon}$, and Σ represents a generic or dummy surface on which sources reside. The "o" superscript simply indicates that the quantity so identified pertains to the exterior model as opposed to the interior model. Expressions for $\mathcal{E}^o[\mathbf{M};\mathbf{r};\Sigma]$ and $\mathcal{H}^o[\mathbf{M};\mathbf{r};\Sigma]$ are similar to those in (11)–(13) but with μ, ε, k, and η replaced by μ_o, ε_o, k_o, and η_o, respectively. The minus (plus) superscripts in (10) indicates that the tangential magnetic field be evaluated in the limit as the field point $\mathbf{r}$ approaches the surface electric current from the interior (exterior) region of either model. Such precaution is not needed in the case of a tangential component of electric field because it is not discontinuous at a surface electric current.

Again we consider the slotted cylinder depicted in [1, Fig. 2]. Because the cylinder is excited by an E-polarized incident plane wave, the induced equivalent electric currents $\mathbf{J}$ and $\mathbf{J}^o$ are z directed. Consequently, $\nabla_s\cdot\mathbf{J}$ and $\nabla_s\cdot\mathbf{J}^o$ are zero forcing the scalar potential terms of (7) through (9) to be zero. Hence, these equations for the slotted cylinder become

$$\frac{k\eta}{4}\int_{C_S+C_A} J_z(\boldsymbol{\rho}')H_0^{(2)}(k|\boldsymbol{\rho}-\boldsymbol{\rho}'|)\,dl' = 0, \quad \boldsymbol{\rho}\in C_S \tag{14}$$

$$\frac{k_o\eta_o}{4}\int_{C_S+C_A} J^o_z(\boldsymbol{\rho}')H_0^{(2)}(k_o|\boldsymbol{\rho}-\boldsymbol{\rho}'|)\,dl' = E^i_z(\boldsymbol{\rho}), \quad \boldsymbol{\rho}\in C_S \tag{15}$$

$$-\frac{k\eta}{4}\int_{C_S+C_A} J_z(\boldsymbol{\rho}')H_0^{(2)}(k|\boldsymbol{\rho}-\boldsymbol{\rho}'|)\,dl' + \frac{k_o\eta_o}{4}\int_{C_S+C_A} J^o_z(\boldsymbol{\rho}')H_0^{(2)}(k_o|\boldsymbol{\rho}-\boldsymbol{\rho}'|)\,dl' = E^i_z(\boldsymbol{\rho}), \quad \boldsymbol{\rho}\in C_A \tag{16}$$

and

$$-\frac{1}{2}J_z(\boldsymbol{\rho}) + \frac{k}{4j}\int_{C_S+C_A} J_z(\boldsymbol{\rho}')\cos\theta H_1^{(2)}(k|\boldsymbol{\rho}-\boldsymbol{\rho}'|)\,dl' - \frac{1}{2}J^o_z(\boldsymbol{\rho}) - \frac{k_o}{4j}\int_{C_S+C_A} J^o_z(\boldsymbol{\rho}')\cos\theta H_1^{(2)}(k_o|\boldsymbol{\rho}-\boldsymbol{\rho}'|)\,dl' = H^i_l(\boldsymbol{\rho}), \quad \boldsymbol{\rho}\in C_A. \tag{17}$$

Note that (14)–(17) appear to be four equations in two unknowns, but this is not the case as is clear if one distinguishes $\mathbf{J}$ and $\mathbf{J}^o$ over C_S from the current over C_A:

$$\mathbf{J} = \begin{cases} \mathbf{J_s}, & \boldsymbol{\rho}\in C_S \\ \mathbf{J_a}, & \boldsymbol{\rho}\in C_A \end{cases} \tag{18}$$

and

$$\mathbf{J^o} = \begin{cases} \mathbf{J^o_s}, & \boldsymbol{\rho}\in C_S \\ \mathbf{J^o_a}, & \boldsymbol{\rho}\in C_A \end{cases}. \tag{19}$$

Once the interior and exterior equivalent currents are determined from solutions of (14)–(17), the correct interior and exterior fields can be computed from the appropriate model. Appealing to the interior model, one employs the interior equivalent current found in (14)–(17) to compute the correct interior field

$$E^{\text{pen}}_z(\boldsymbol{\rho}) = -\frac{k\eta}{4}\int_{C_S+C_A} J_z(\boldsymbol{\rho}')H_0^{(2)}(k|\boldsymbol{\rho}-\boldsymbol{\rho}'|)\,dl'. \tag{20}$$

III. Numerical Scheme

In this section, schemes for converting the integral equations into matrix equations are presented. The first step in the numerical method [6] is to discretize the geometry and approximate the unknown electric current over the contour. The current is expanded in a linear combination of basis functions and the equations are tested in order to obtain an adequate number of equations to solve for the unknown coefficients of the basis functions.

A. Scatterer Method

We discretize the contour C_S into N straight-line subsections ΔC_n that approximate the original contour and approximate J_z by a linear combination of N piecewise constant functions with unknown current coefficients $\{J_n\}$. Collocation at the match points $\boldsymbol{\rho}_m$ located at the subcontour centers yields

$$\frac{k\eta}{4}\sum_{n=1}^{N} J_n\int_{\Delta C_n} H_0^{(2)}(k|\boldsymbol{\rho}_m-\boldsymbol{\rho}'|)\,dl' = E^i_z(\boldsymbol{\rho}_m), \quad m = 1,2,\cdots,N \tag{21}$$

which can be written in matrix form as

$$[Z_{mn}][J_n] = [V_m] \tag{22}$$

where $[J_n]$ is a column vector containing the unknown coefficients, $[Z_{mn}]$ is a matrix whose elements are

$$Z_{mn} = \frac{k\eta}{4}\int_{\Delta C_n} H_0^{(2)}(k|\boldsymbol{\rho}_m - \boldsymbol{\rho}'|)\,dl' \tag{23}$$

and $[V_m]$ is a column vector whose elements are values on the right-hand side of (21)

$$V_m = E_z^i(\boldsymbol{\rho}_m) = E_o^i e^{jk(x_m\cos\phi^i + y_m\sin\phi^i)} \tag{24}$$

where x_m and y_m are the Cartesian coordinates of $\boldsymbol{\rho}_m$. Since ΔC_n is a straight-line subsection, one may replace $\boldsymbol{\rho}'$ by $\boldsymbol{\rho}_n + l'\hat{\mathbf{l}}_n$ and write (23) as

$$Z_{mn} = \frac{k\eta}{4}\int_{-\Delta l_n/2}^{\Delta l_n/2} H_0^{(2)}(k|\boldsymbol{\rho}_m - \boldsymbol{\rho}_n - l'\hat{\mathbf{l}}_n|)\,dl' \tag{25}$$

where Δl_n is the length of the nth straight-line segment and $\hat{\mathbf{l}}_n$ is a unit vector along the nth straight-line subsection ΔC_n in the direction of increasing arc displacement l.

The scattered field can be computed by integrating over the induced current obtained from the integral equation solution

$$E_z^s(\boldsymbol{\rho}) = -\frac{k\eta}{4}\sum_{n=1}^{N} J_n \int_{-\Delta l_n/2}^{\Delta l_n/2} H_0^{(2)}(k|\boldsymbol{\rho} - \boldsymbol{\rho}_n - l'\hat{\mathbf{l}}_n|)\,dl'. \tag{26}$$

The total field everywhere is

$$\hat{\mathbf{z}}E_z(\boldsymbol{\rho}) = \hat{\mathbf{z}}E_z^s(\boldsymbol{\rho}) + \hat{\mathbf{z}}E_z^i(\boldsymbol{\rho}) \tag{27}$$

where $\boldsymbol{\rho}$ is the observation point of interest.

B. Short-Circuit Current Method

With a minor modification the numerical scheme used to implement the scatterer method can be employed in the short-circuit current method. One solves (2) or (3) using the method outlined above to determine the short-circuit current on the cylinder. The matrix equation for this method can be written differently from (22) as

$$\begin{bmatrix} [Z_{mn}^{aa}] & [Z_{mn}^{as}] \\ [Z_{mn}^{sa}] & [Z_{mn}^{ss}] \end{bmatrix} \begin{bmatrix} [J_n^a] \\ [J_n^s] \end{bmatrix} = \begin{bmatrix} [V_m^a] \\ [V_m^s] \end{bmatrix} \tag{28}$$

where $[J_n^a]$ and $[J_n^s]$ are the unknown current coefficients over the aperture and conductor surfaces, respectively, and where the matrix elements $[Z_{mn}^{aa}]$, $[Z_{mn}^{as}]$, $[Z_{mn}^{sa}]$, and $[Z_{mn}^{ss}]$ represent the contributions from the shorted aperture to itself, the conductor to the shorted aperture, the shorted aperture to the conductor and the conductor to itself, respectively. $[V_m^a]$ and $[V_m^s]$ are the values of the right-hand side of (2). If the combined field formulation of (3) is needed for accuracy, (28) would be appropriately modified.

Once the short-circuit current has been found, the equivalent E-field excitation $\mathbf{E}^{\text{imp}}$ is found from

$$E_z^{\text{imp}}(\boldsymbol{\rho}) = -\frac{k\eta}{4}\sum_{n=1}^{N^a} J_n^{\text{imp}} \int_{-\Delta l_n/2}^{\Delta l_n/2} H_0^{(2)}(k|\boldsymbol{\rho} - \boldsymbol{\rho}_n - l'\hat{\mathbf{l}}_n|)\,dl' \tag{29}$$

where J^{imp} is the impressed current used in (5) to determine the induced current on the "scatterer." This is conveniently written in matrix form as

$$[Z_{mn}^{ss}][J_n] = -[Z_{mn}^{sa}][J_n^{\text{imp}}] \tag{30}$$

where $[J_n]$ is the induced current, where $[J_n^{\text{imp}}]$ is the known impressed current, equal, and opposite to the aperture short-circuit current ($J^{\text{imp}} = -J^{\text{sc}}$) and where the right-hand side of (30) is the z component of the equivalent E-field excitation evaluated at the points $\boldsymbol{\rho}_m$.

The penetrated field is simply the summation of the field due to the equivalent induced current on the conductor and that due to the impressed current in the aperture

$$\begin{aligned} E_z^{\text{pen}}(\boldsymbol{\rho}) = &-\frac{k\eta}{4}\sum_{n=1}^{N^s} J_n \int_{-\Delta l_n/2}^{\Delta l_n/2} H_0^{(2)}(k|\boldsymbol{\rho} - \boldsymbol{\rho}_n - l'\hat{\mathbf{l}}_n|)\,dl' \\ &-\frac{k\eta}{4}\sum_{n=1}^{N^a} J_n^{\text{imp}} \int_{-\Delta l_n/2}^{\Delta l_n/2} H_0^{(2)}(k|\boldsymbol{\rho} - \boldsymbol{\rho}_n - l'\hat{\mathbf{l}}_n|)\,dl' \end{aligned} \tag{31}$$

where N^s and N^a are the numbers of current unknowns on the cylinder and in the aperture, respectively.

C. Equivalent Current Method

Following the procedure in Section III-B above, we expand the equivalent electric currents in (14)–(17) in linear combinations of piecewise constant functions and enforce the new equations at match points $\boldsymbol{\rho}_m$ located at the subcontour centers

$$\frac{k\eta}{4}\sum_{n=1}^{N^s+N^a} J_n \int_{\Delta C_n} H_0^{(2)}(k|\boldsymbol{\rho}_m - \boldsymbol{\rho}'|)\,dl' = 0, \quad m = 1, 2, \cdots, N^s \tag{32}$$

$$\frac{k_o\eta_o}{4}\sum_{n=1}^{N^a+N^s} J_n^o \int_{\Delta C_n} H_0^{(2)}(k_o|\boldsymbol{\rho}_m - \boldsymbol{\rho}'|)\,dl' = E_z^i(\boldsymbol{\rho}_m), \quad m = 1, 2, \cdots, N^s \tag{33}$$

$$\begin{aligned} -\frac{k\eta}{4}&\sum_{n=1}^{N^a+N^s} J_n \int_{\Delta C_n} H_0^{(2)}(k|\boldsymbol{\rho}_m - \boldsymbol{\rho}'|)\,dl' \\ &+ \frac{k_o\eta_o}{4}\sum_{n=1}^{N^a+N^s} J_n^o \int_{\Delta C_n} H_0^{(2)}(k_o|\boldsymbol{\rho}_m - \boldsymbol{\rho}'|)\,dl' = E_z^i(\boldsymbol{\rho}_m), \\ &m = N^s+1, N^s+2, \cdots, N^s+N^a \end{aligned} \tag{34}$$

and

$$\begin{aligned} -\frac{J_m}{2} &+ \sum_{n=1}^{N^s+N^a} J_n \frac{k}{4j}\int_{\Delta C_n} \cos\theta_m H_1^{(2)}(k|\boldsymbol{\rho}_m - \boldsymbol{\rho}'|)\,dl' \\ -\frac{J_m^o}{2} &- \sum_{n=1}^{N^s+N^a} J_n^o \frac{k_o}{4j}\int_{\Delta C_n} \cos\theta_m H_1^{(2)}(k_o|\boldsymbol{\rho}_m - \boldsymbol{\rho}'|)\,dl' \\ &= H_l^i(\boldsymbol{\rho}_m), \quad m = N^s+1, N^s+2, \cdots, N^s+N^a \end{aligned} \tag{35}$$

in which $\cos\theta_m = \hat{\mathbf{u}}(\boldsymbol{\rho}_m)\cdot\hat{\mathbf{n}}(\boldsymbol{\rho}_m)$, while $-\frac{J_m}{2}$ represents the field contribution of the basis function at $\boldsymbol{\rho}_m$ due to J_m (more

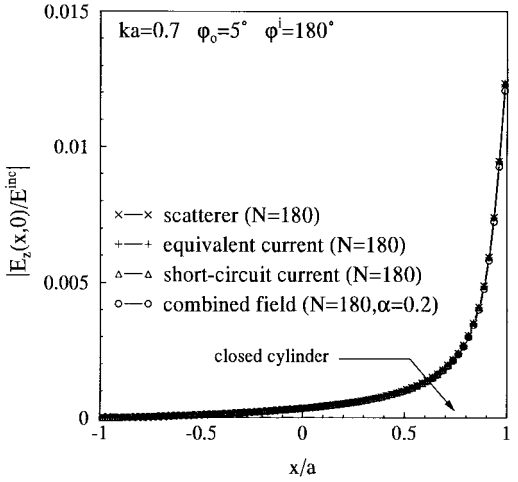

Fig. 3. Magnitude of axially directed (normalized) electric field on x axis of slotted circular cylinder excited by TM$_z$ plane wave [$ka = 0.7$, $\phi_o = 5°$, $\phi^i = 180°$].

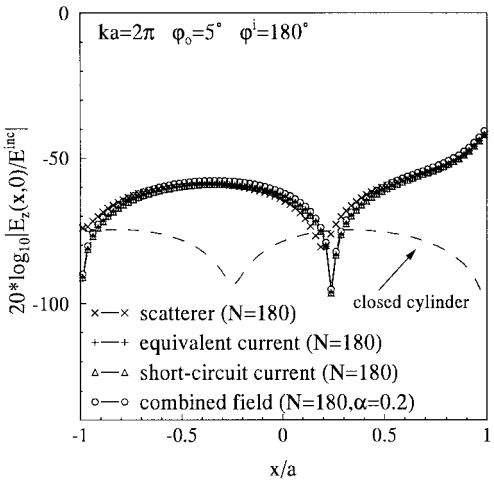

Fig. 5. Magnitude of axially directed (normalized) electric field on x axis of slotted circular cylinder excited by TM$_z$ plane wave [$ka = 2\pi$, $\phi_o = 5°$, $\phi^i = 180°$].

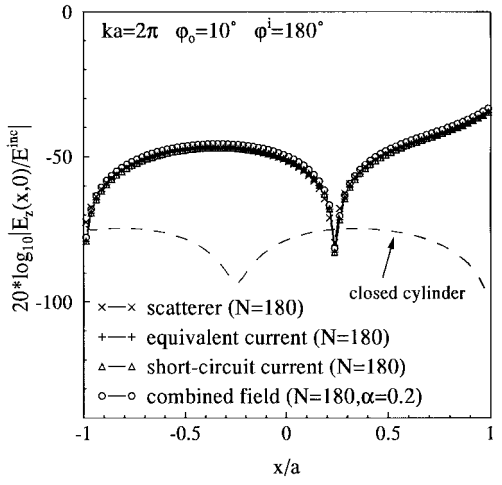

Fig. 4. Magnitude of axially directed (normalized) electric field on x axis of slotted circular cylinder excited by TM$_z$ plane wave [$ka = 2\pi$, $\phi_o = 10°$, $\phi^i = 180°$].

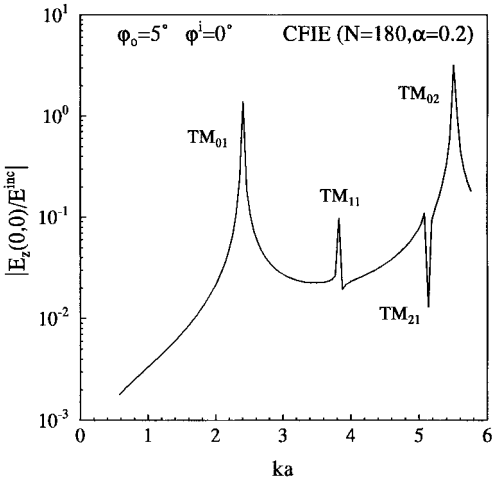

Fig. 6. Magnitude of axially directed (normalized) electric field at center of-slotted circular cylinder excited by TM$_z$ plane wave for various ka[$\phi_o = 5°$, $\phi^i = 0°$].

precisely, due to the product of J_m and the basis function centered at $\boldsymbol{\rho}_m$). The penetrated field is then determined from the interior equivalent currents from

$$E_z^{\text{pen}}(\boldsymbol{\rho}) = -\frac{k\eta}{4}\sum_{n=1}^{N^s+N^a} J_n \int_{-\Delta l_n/2}^{\Delta l_n/2} H_0^{(2)}(k|\boldsymbol{\rho}-\boldsymbol{\rho}_n - l'\hat{\mathbf{1}}_n|)\, dl'. \tag{36}$$

IV. Results and Discussion

Computer codes have been written to implement the various methods presented in Sections II and III, and the currents determined from the codes have been checked in special cases against known solutions or published data. Early work in determining the electric field penetration into slotted conducting circular cylinders is due to Senior [7], whose results have been reproduced with high accuracy by the present methods. Senior's results are for moderately wide slots ($\phi_o = 10°$ and $\phi_o = 30°$), so any of the methods discussed in Sections II and III should yield accurate penetrated field. Mautz and Harrington [8] determine the field amplitude $|E_z|$ at the center of the cylinder as a function of ka for $\phi_o = 10°$ and $30°$ and $\phi^i = 0°$. Fig. 9 of their paper [8] is reproduced with excellent accuracy for $\phi_o = 10°$ and $ka \leq 4$ in Fig. 6 of this work and is extended to include $4.0 \leq ka \leq 6.0$.

We select as sample structures the axially slotted circular conducting cylinder and axially slotted rectangular conducting cylinder excited by TM (to cylinder and slot axes) incident plane waves to illustrate the methods of this paper and their relative accuracies. A cross-sectional view of the slotted circular cylinder is found in [1, Fig. 2] from which one observes that the cylinder radius is a, that the slot subtends an angle $2\phi_o$, and that an axially independent plane wave is incident at an angle ϕ^i measured with respect to the x-axis. A cross-sectional view of the slotted rectangular cylinder is shown in [1, Fig. 5]. The cylinder length is $2s$, the cylinder

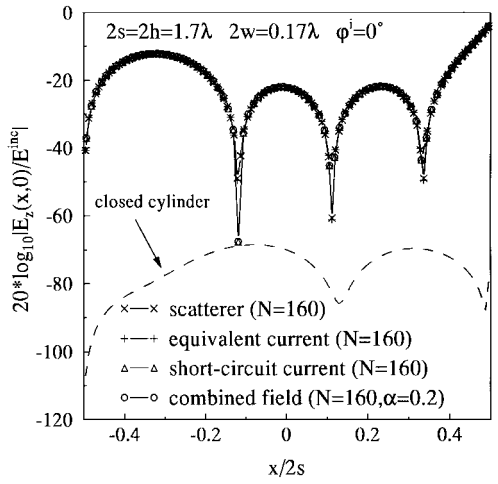

Fig. 7. Magnitude of axially directed (normalized) electric field on x axis of slotted square cylinder excited by TM_z plane wave [$2s = 2h = 1.7\lambda$, $2w = 0.17\lambda$, $\phi^i = 0°$].

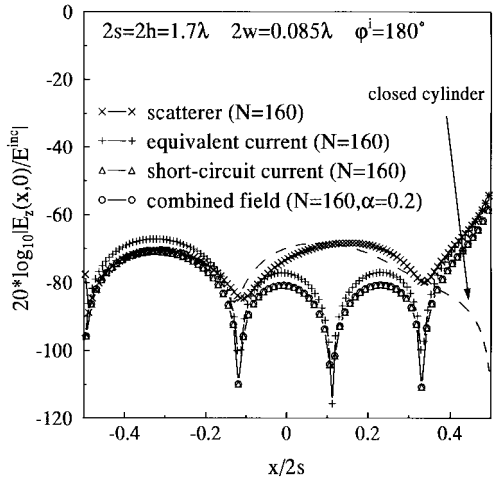

Fig. 8. Magnitude of axially directed (normalized) electric field on x axis of square cylinder excited by TM_z plane wave [$2s = 2h = 1.7\lambda, 2w = 0.085\lambda$, $\phi^i = 180°$].

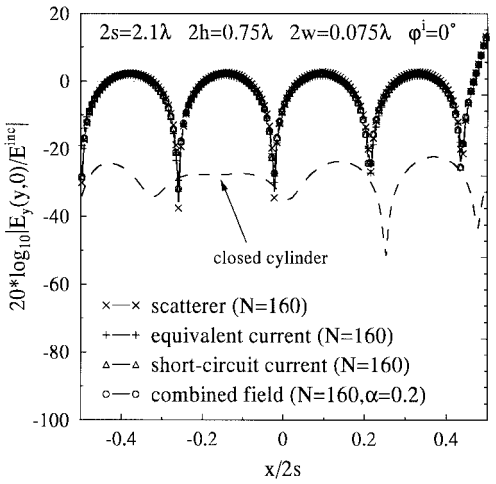

Fig. 9. Magnitude of axially directed (normalized) electric field on x axis of slotted rectangular cylinder excited by TM_z plane wave [$2s = 2.1\lambda$, $2h = 0.75\lambda$, $2w = 0.075\lambda$, $\phi^i = 0°$].

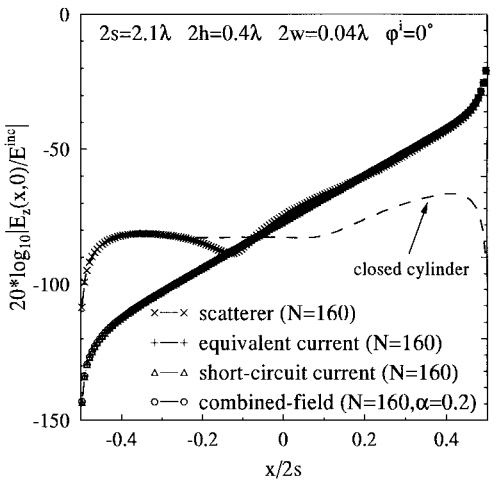

Fig. 10. Magnitude of axially directed (normalized) electric field on x axis of slotted rectangular cylinder excited by TM_z plane wave [$2s = 2.1\lambda, 2h = 0.4\lambda, 2w = 0.04\lambda, \phi^i = 0°$].

height is $2h$, the slot width is $2w$, and an axially independent plane wave is incident upon the slotted cylinder at an angle ϕ^i measured with respect to the x axis.

Figs. 2 and 3 give the magnitude of axially directed normalized electric field along the x axis of the slotted circular cylinder excited by a plane wave for $(\phi_o = 10°, \phi^i = 0°)$ and $(\phi_o = 5°, \phi^i = 180°)$, respectively. Very close agreement is seen for the values of penetrated field calculated by means of the scatterer method, equivalent current method, short-circuit current method, and combined field short-circuit current method for this small cylinder. In order to establish a reference value for the noise floor of the solution, identified in the figures as "closed cylinder," the axially directed normalized electric field along the x axis of a *closed* circular cylinder $(ka = 0.7)$ subject to a TM_z incident plane wave $(\phi^i = 0°)$ is determined from a solution of the EFIE. In all cases these values should be zero. The value of the interior field of the closed cylinder is not discernible from the value zero in Figs. 2 and 3. Values of N in the figures indicate the number of unknowns employed to obtain a given solution and α is the value of the "combined field solution parameter" of (3).

As in the TE case, if the diameter of the circular cylinder is increased to $2a = 2\lambda$ $(ka = 2\pi)$, we again see that the interior field exhibits greater spatial variation different from that observed in the smaller cylinder cases. The log magnitude of the axially-directed electric field along the x axis of a $ka = 2\pi$ slotted circular cylinder excited by a $\phi^i = 180°$ incident plane wave is presented in Figs. 4 and 5. When the slot is relatively large $(\phi_o = 10°)$, good agreement among data obtained from all methods is observed. However, if the angle is decreased to $\phi_o = 5°$, the penetrated field determined by the scatterer method disagrees with that of the other methods.

When the interior field is very small comparable to the noise floor of the problem (closed cylinder values), the accuracy of the values obtained by the scatterer method may be very poor. An example of this can be seen in Fig. 5 where, for a $ka = 2\pi$ slotted circular cylinder with angle $\phi_o = 5°$, the values of the penetrated field calculated by means of the

equivalent current method, short-circuit method, and combined field short-circuit method are very close in value, but the scatterer method fails to yield the correct penetrated field because the scattered electric field produced by the induced current on the cylinder and the incident electric field are almost of the same magnitude but opposite in sign. A more dramatic example of *subtractive cancellation* error is found in the square and rectangular cylinder data of Figs. 8 and 10.

In Fig. 6 the field amplitude of the axially directed normalized electric field at the center of the circular cylinder is displayed as a function of ka for $\phi_o = 5^\circ$ and $\phi^i = 0^\circ$. The TM_{01} mode manifests itself at $ka = 2.405$, the TM_{11} mode at $ka = 3.832$, the TM_{21} mode at $ka = 5.136$, and the TM_{02} mode at $ka = 5.520$.

In Fig. 7, is displayed the penetrated field for a slotted square cylinder with $2s = 2h = 1.7\lambda$ and $2w = 0.17\lambda$ excited by a TM_z plane wave ($\phi^i = 0^\circ$). The results from the different methods are in good agreement. However, if the incident angle is changed to $\phi^i = 180^\circ$ and the slot width is decreased to $2w = 0.085\lambda$, as seen in Fig. 8, the field penetration determined by the scatterer method is inaccurate. The field predicted by the scatterer method is bounded by the noise floor at the precision used.

In Fig. 9 is displayed the interior field distribution for a rectangular cylinder with $2s = 2.1\lambda$, $2h = 0.75\lambda$, $2w = 0.075\lambda$, and incident field angle $\phi^i = 0^\circ$. Since this structure can be viewed as a shorted parallel-plate guide operating above cutoff for the TM_1 mode, standing wave patterns due to waves traveling in the positive and negative x directions can be clearly seen. In Fig. 10, the field distribution in a rectangular cylinder with $2s = 2.1\lambda$, $2h = 0.4\lambda$, $2w = 0.04\lambda$, and incident field angle $\phi^i = 0^\circ$ is shown. Since this guide operates below the TM cutoff *and* because there is no TEM mode (in the x-direction) in the guide, there is no standing wave pattern.

REFERENCES

[1] J. D. Shumpert and C. M. Butler, "Penetration through slots in conducting cylinders—Part 1: TE case," *IEEE Trans. Antennas Propagat.*, this issue, pp. 1611-1620.

[2] S. A. Schelkunoff, "Kirchhoff's formula, its vector analogue and other field equivalence theorems," *Commun. Pure Appl. Math.*, vol. 4, pp. 43–59, June 1951.

[3] J. R. Mautz and R. F. Harrington, "H-field, E-field, and combined-field solutions for conducting bodies of revolution," *AEÜ*, vol. 32, pp. 157–164, 1978.

[4] N. Morita, N. Kumagai, and J. R. Mautz, *Integral Equation Methods in Electromagnetics*. Boston: Artech House, 1990.

[5] R. F. Harrington, *Time-Harmonic Electromagnetic Fields*. New York: McGraw-Hill, 1961.

[6] ———, *Field Computation by Moment Methods*. Piscataway, NJ: IEEE Press, 1993.

[7] T. B. A. Senior, "Electromagnetic field penetration into a cylindrical cavity," *IEEE Trans. Electromagn. Compat.*, vol. EMC-18, pp. 71–73, May 1976.

[8] J. R. Mautz and R. F. Harrington, "Electromagnetic penetration into a conducting circular cylinder through a narrow slot, TM case," *J. Electromagn. Waves Applicat.*, vol. 2, nos. 3/4, pp. 269–293, 1988.

John D. Shumpert (S'89), for a biography, see this issue, p. 1620.

Chalmers M. Butler (S'55–M'63–SM'75–F'83), for a photograph and biography, see p. 1644 of the November 1997 issue of this TRANSACTIONS.